

Growth of Mesoscale Ordered Two-Dimensional Hydrogen-Bond Organic Framework with the Observation of Flat Band

Minghu Pan^{1,2,*}, Xin Zhang^{3,*}, Yinong Zhou^{4,*}, Pengdong Wang^{5,*}, Qi Bian², Hang Liu⁴, Xingyue Wang¹, Xiaoyin Li⁴, Aixi Chen⁵, Xiaoxu Lei⁵, Shaojian Li², Zhengwang Cheng⁶, Zhibin Shao¹, Haoxuan Ding⁷, Jianzhi Gao^{1,‡}, Fangsen Li^{5,§}, and Feng Liu^{4,||}

¹*School of Physics and Information Technology, Shaanxi Normal University, Xi'an 710119, China*

²*School of Physics, Huazhong University of Science and Technology, Wuhan 430074, China*

³*School of Physics, Northwest University, Xi'an, 710069, China*

⁴*Department of Materials Science and Engineering, University of Utah, Salt Lake City, Utah 84112, USA*

⁵*Vacuum Interconnected Nanotech Workstation, Suzhou Institute of Nano-Tech and Nano-Bionics, Chinese Academy of Sciences (CAS), Suzhou 215123, China*

⁶*School of Science and Hubei Engineering Technology Research Center of Energy Photoelectric Device and System, Hubei University of Technology, Wuhan 430068, China*

⁷*School of Physics and Astronomy, University of Birmingham, Birmingham, B15 2TT, United Kingdom*

 (Received 7 September 2022; revised 18 November 2022; accepted 16 December 2022; published 20 January 2023)

Flat bands (FBs), presenting a strongly interacting quantum system, have drawn increasing interest recently. However, experimental growth and synthesis of FB materials have been challenging and have remained elusive for the ideal form of monolayer materials where the FB arises from destructive quantum interference as predicted in 2D lattice models. Here, we report surface growth of a self-assembled monolayer of 2D hydrogen-bond (H-bond) organic frameworks (HOFs) of 1,3,5-tris(4-hydroxyphenyl) benzene (THPB) on Au(111) substrate and the observation of FB. High-resolution scanning tunneling microscopy or spectroscopy shows mesoscale, highly ordered, and uniform THPB HOF domains, while angle-resolved photoemission spectroscopy highlights a FB over the whole Brillouin zone. Density-functional-theory calculations and analyses reveal that the observed topological FB arises from a hidden electronic breathing-kagome lattice without atomically breathing bonds. Our findings demonstrate that self-assembly of HOFs provides a viable approach for synthesis of 2D organic topological materials, paving the way to explore many-body quantum states of topological FBs.

DOI: [10.1103/PhysRevLett.130.036203](https://doi.org/10.1103/PhysRevLett.130.036203)

Introduction.—A topological flat band (FB) presents an exotic Bloch state without band dispersion. It arises from destructive interference (phase cancellation) of Bloch wave functions, such as materials with a kagome lattice [1–3] or more generally line-graph lattice models [1–9], differing from topologically trivial FBs of highly localized atomic orbitals, such as *f* orbitals [10] and dangling bonds [11], and the FBs resulted from moiré band folding of twisted bilayer graphene [12]. The phase cancellation renders the FB to be topological in both real space characterized with compact localized state [3] and momentum space having a singular touching point with a dispersive band [4,5]. Also, the completely quenched electron kinetic energy in a FB magnifies electron-electron interaction, leading to a range of theoretically predicted many-body quantum phases, such as fractional quantum Hall effect [7], Wigner crystallization [13], ferromagnetism [3,14], superconductivity [15], and excitonic insulator [16]. Recent discovery of superconductivity in twisted bilayer graphene has further boosted the interest in FBs [17].

On the other hand, various 2D FB materials have been predicted from first principles. These include 2D metal-organic frameworks (MOFs) [18–21], covalent organic frameworks (COFs) [14,22–25], hydrogen-bond (H-bond) organic frameworks (HOFs) [26], and inorganic 2D materials [27]. Experimentally, FB features have been observed in the surface of transition-metal kagome compounds [28–33], twisted bilayer graphene [34], and heterostructure [35], all having a layered structure which contains one atomic layer manifesting a 2D FB lattice model, such as kagome lattice. But in these systems the FB is inevitably overlapping with many dispersive bands from other atomic layers. In general, experimental realization of topological FBs has been challenging due to the lack of FB materials, especially elusive in the ideal form of monolayer materials originally proposed based on 2D lattice models. To date, there is no monolayer material that has been synthesized to enable direct observation of FB. A recent experiment has successfully grown COF monolayers of tribromotrioxaazatriangulene and tribromotrioxoazatriangulene on Au(111)

substrate [36], enabling a clear observation of Dirac bands by angle-resolved photoemission spectroscopy (ARPES); however, the FB, which was supposed to be present with a kagome sublattice [36], cannot be directly observed because it is located ~ 1.0 eV above Fermi level [23].

In this Letter, we report direct observation of FB in a self-assembled monolayer of 2D HOF of 1,3,5-tris(4-hydroxyphenyl)benzene (THPB) on Au(111) surface. Formation of mesoscale, uniform domains of THPB are seen by scanning tunneling microscopy or spectroscopy (STM or STS), whose long-range order and lattice symmetry are further confirmed by low-energy electron diffraction (LEED). Remarkably, a FB over the whole BZ is observed by ARPES. Interestingly, density-functional-theory (DFT) calculations reveal that the FB arises from a hidden *electronic* breathing-kagome sublattice made of corner benzene rings (CBRs) of THPB, and is hence topological nontrivial, but *atomically* all the CBRs locate at the sites of a kagome lattice without breathing bonds. The electronic breathing effect is shown to be caused by different inter-CBR hopping mediated by H bonds versus covalent bonds. Furthermore, the most salient features of H bonds are characterized by high-resolution STM or STS, Raman spectroscopy, and DFT calculations.

Experimental growth and structural characterization.— Instead of realizing FB lattices using MOFs [14–17] and COFs [9,18,19] widely predicted by theory, we take a different approach to grow the less studied HOF, since H bonds are weaker but more flexible than the organometallic and covalent bonds, in an attempt to assemble large-scale monolayer structures of high uniformity. We use THPB as a model molecule which is deposited onto Au(111) substrate at room temperature [see Methods in Supplemental Material (SM) [37] for sample preparation]. The H-bond assisted self-assembly turns out to be very successful as evidenced in Fig. 1. We note that although synthesis and STM imaging of THPB HOF has been reported before [57,58], those structures are mostly nanometer-sized islands, preventing them from ARPES measurement.

Figures 1(a) and 1(b) show large-scale STM images of 2D crystalline domains of THPB monolayer film at a coverage of 0.75 ML (monolayer), where THPB molecules aggregate into a triangle lattice with long-range order. In Fig. 1(b), the crystalline orientations of Au[1 $\bar{1}$ 0] and [11 $\bar{2}$] are determined by visualizing the well-known herringbone reconstruction of Au(111) surface [59]. Domain walls are observed with adjacent domains being mirror symmetric with each other (Fig. S1 in SM [37]). The THPB HOF lattices have been grown successfully over the entire substrate surface and remain intact across surface steps [see Figs. 1(a) and 1(b)].

A high-resolution STM image [Fig. 1(c)] distinguishes each individual THPB molecule consisting of three bright protrusions from three CBRs, and reveals the self-assembled trigonal THPB lattice having a lattice constant

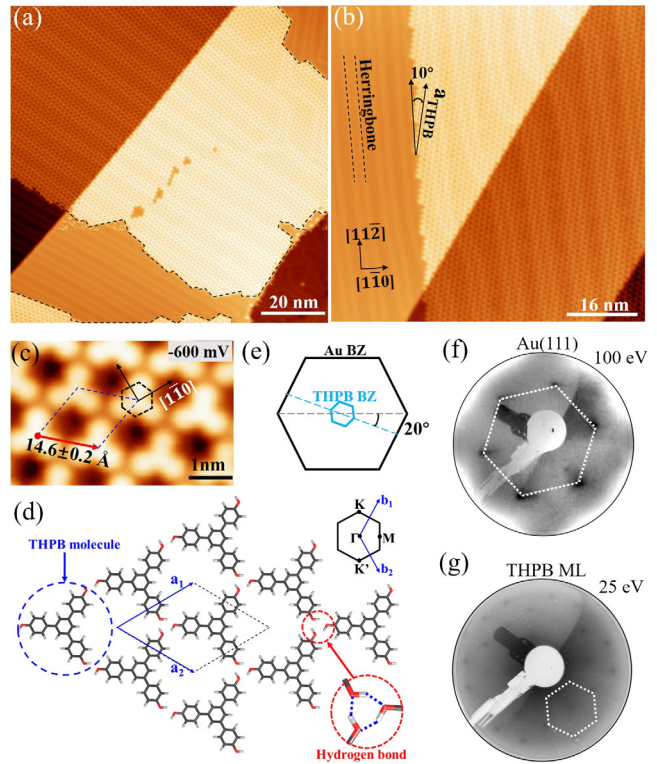


FIG. 1. (a) and (b) Large-scale topographic STM images ($I_t = 200$ pA, $V_b = -0.5$ V). The orientation of HOF is determined whose lattice vector is aligned $\sim 10^\circ$ away from the Au[11 $\bar{2}$] direction. (c) Close-up STM image showing a trigonal lattice with a lattice constant of 14.6 ± 0.2 Å, averaged from line profiles. The dashed hexagon marks the unit cell of Au lattice showing the close-packed [1 $\bar{1}$ 0] direction which has a 20° angle with the THPB HOF lattice vectors. (d) Schematic lattice model indicating three H bonds in between THPB. (e) The relationship between the BZ of Au(111) surface and of HOF. (f) and (g) LEED patterns of clean and HOF-covered Au(111) surface taken at the energies of 100 and 25 eV, respectively. Their reciprocal lattices are marked with white dashed hexagons.

of 14.6 ± 0.2 Å. A schematic lattice model is drawn in Fig. 1(d). The THPB molecules aggregate via formation of three H bonds, rotated by 120° with each other, between the hydroxyl groups at the corner of THPB. The orientation of the THPB HOF lattice is determined whose lattice vectors a_1 (a_2) are aligned $\sim 20^\circ$ from the close-packed [1 $\bar{1}$ 0] direction of the Au surface (see also Fig. S1c in SM [37]). Consequently, the BZ of HOF lattice and of Au(111) surface rotate away from each other by $\sim 20^\circ$, as shown in Fig. 1(e); the former is also ~ 5 times smaller than the latter. These relations are used for analyzing their respective ARPES spectra later.

The long-range order of THPB HOF lattice is further confirmed by LEED, displaying diffraction spots from a periodic superstructure [Fig. 1(g)]. It confirms the HOF domains are aligned in the same orientation, with a trigonal lattice rotated by 20° from that of the Au(111) surface

[Fig. 1(f)]. The lattice constant of HOF is extracted to be ~ 1.5 nm from LEED, in very good agreement with STM. These findings demonstrate that epitaxial growth of 2D HOFs offers a viable approach to synthesize organic 2D materials, especially monolayer HOFs with desirable electronic properties, such as the FB, as demonstrated below.

ARPES observation of flat band.—Importantly, the mesoscale size and mono-orientation of 2D THPB HOF has enabled characterization of its band structure by ARPES, which has been used to investigate band structure of other organic systems [60–62]. As a reference, the ARPES of bare Au(111) surface was measured first [Fig. 2(a)]. The well-known Shockley surface states with a parabolic valley at -0.5 eV are observed. In addition, the parabolic Au surface *sp* band having the bottom of valley at ~ -3.6 eV and some bulk bands lying at the lower energies are also visible, in agreement with previous reports [63,64]. The *d* band of Au locates below -3.8 eV.

We have grown 2D THPB HOFs from ~ 0.5 ML to nearly full coverage on Au(111) surface with their long-range order all confirmed by STM and LEED. Figure 2(b) shows the ARPES measured from one of the 0.5 ML samples, along the $K_{\text{Au}}-\Gamma-K_{\text{Au}}$ direction of the Au(111) BZ. Remarkably, a FB is seen at the energy of -2.62 eV (see also the second-derivative intensity plot in the middle panel). The Au Shockley surface state is no longer visible upon molecular coverage, while its *sp* surface bands and bulk *d* bands become weaker. The FB gives rise to a distinct peak in the density of state (DOS) (right) which is absent in the DOS of bare Au [Fig. 2(a)]. Considering Au HOF forming a metal-semiconductor heterojunction and assuming the Fermi level of Au is aligned with the midgap position of HOF, the position of FB at -2.62 eV sets a lower limit for the band gap of HOF to be 5.24 eV (see band diagram in Fig. S2 [37]). The other DOS peaks in the

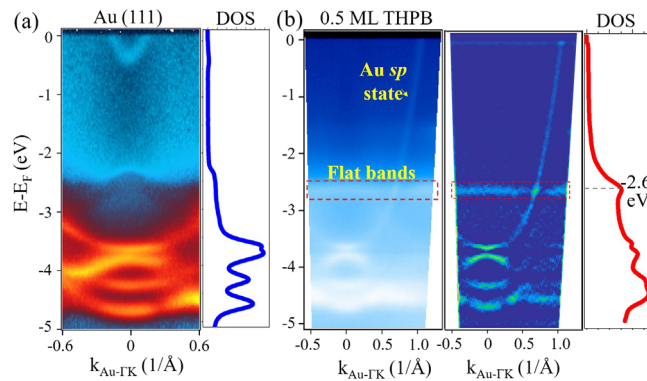


FIG. 2. (a) The photoemission intensity plot of E_B-k_x cut along the $K_{\text{Au}}-\Gamma-K_{\text{Au}}$ direction at $k_y = 0$ (left) and the integrated DOS from ARPES (right), taken from the bare Au(111) surface. K_{Au} is the K point of Au(111) surface BZ. (b) The ARPES spectra (left), the second-derivative plot (middle), and the integrated DOS from the ARPES showing a peak at the FB energy of -2.62 eV (right), taken along $\Gamma-K_{\text{Au}}$ direction from a 0.5 ML THPB film.

right-hand panel of Fig. 2(b), e.g., -3.9 eV, are aligned well with the top or bottom of some parabolic bands from Au *sp* and bulk states.

To confirm the FB exists in the whole 2D BZ, we also conducted low-temperature ARPES measurement at 12 K on a sample of nearly full coverage of THPB HOF. The constant-energy contour (CEC) at -2.67 eV is shown in Fig. 3(a), which signifies the presence of the circular Au *sp* band appearing near the BZ boundary. Furthermore, to reveal the truly flatness of FB, three line cuts are taken along momentum paths of $\Gamma-K_{\text{HOF}}$, $\Gamma-K_{\text{Au}}$, and

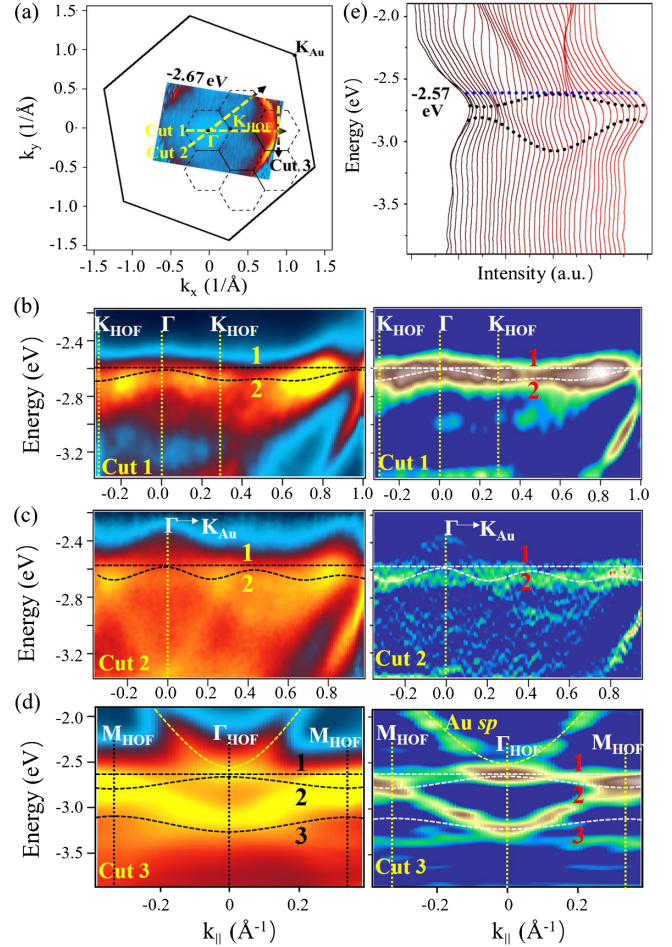


FIG. 3. (a) The CEC measured at -2.67 eV and 12 K. The states of Au *sp* bands are clearly visible near the BZ boundary (half circle). The yellow dashed lines indicate three line cuts taken for ARPES measurements in (b)–(d). (b) High-resolution ARPES (left) and second-derivative (right) plots measured at 12 K from cut 1 along the $\Gamma-K_{\text{HOF}}$ direction as marked in (a). (c) Same as (b) for cut 2 along $\Gamma-K_{\text{Au}}$. (d) Same as (b) for cut 3 along $M_{\text{HOF}}-\Gamma_{\text{HOF}}-M_{\text{HOF}}$. K_{HOF} , Γ_{HOF} , and M_{HOF} are special k points in the BZ of THPB HOF. The dashed black lines are the DFT LDA Wannier bands superimposed on the experimental spectra. (e) The EDC of (d). The blue and black dotted lines denote the peak positions obtained by Gaussian fitting, representing bands 1, 2, and 3. The FB (band 1) locates at -2.57 eV.

$M_{\text{HOF}}-\Gamma-M_{\text{HOF}}$, as indicated by yellow dashed lines in Fig. 3(a). Cut 1 [Fig. 3(b)] and 2 [Fig. 3(c)] are taken with the energies from -2.2 to -3.4 eV. Both intensity (left) and second-derivative (right) plots of cut 1 and 2 show a FB (band 1) at -2.62 eV, indicating it touches with a weakly dispersive band (band 2) at the Γ point, as the theory would predict (dashed lines). There is also a parabolic Au surface sp band that intersects with these two HOF bands. Two entangled bands can be distinguished more clearly in the spectrum of cut 3 [Fig. 3(d)], and interestingly, a third strongly dispersive band shows up below the abovementioned two bands. This third band is further confirmed by the energy distribution curves (EDCs) measured from -0.39 to 0.39 \AA^{-1} [Fig. 3(e)]. By deconvoluting these three bands, the FB energy is resolved at -2.57 eV, slightly different from its apparent position of -2.62 eV in Fig. 2(b). Overall, the band dispersions are clearer in Fig. 3(d) than those in Figs. 3(b) and 3(c), partly because cut 3 is outside the circular Au sp band at the BZ boundary [Fig. 3(a)], so that the Au sp band sits above without overlapping with the FB. More line-cut spectra are available in Fig. S3 in SM [37].

Topological FBs from a hidden breathing-kagome sublattice.—The THPB HOF has an apparent triangle lattice, as shown in Fig. 1(d), which is not expected to host FB. To reveal the origin of the observed FB, we have performed DFT calculations. The optimized lattice structure and the calculated band structure are shown in Figs. 4(a) and 4(b), respectively. The THPB HOF is a semiconductor having a FB below the Fermi level as the valence band maximum [Fig. 4(b)], consistent with the experiment [Figs. 2(b) and S2 in SM [37]]. We note that the calculated gap of ~ 3.0 eV from local-density approximation (LDA) is corrected to ~ 4.0 eV by the Heyd-Scuseria-Ernzerhof (HSE) functional, which is still ~ 1.0 eV smaller than the experimental value in Fig. 2(b). This is reasonable considering there could be some charge transfer from Au surface to HOF to shift the Fermi level of HOF above its midgap position and the HSE gap may still be an underestimation [65]. We also made calculations using the van der Waals functional (DFT D2) to better treat H bonds, which did not show a significant difference.

Figure 4(b) shows that the FB touches with a dispersive band below, as observed. A checkerboard lattice could have such a two-band configuration [66], but the THPB HOF lattice does not have a square lattice symmetry. Therefore, also the lower lying dispersive band, observed in ARPES as well [band 3 in Fig. 3(d)], has to be considered in the analysis. This led us to realize that it resembles the typical three-bands structure of a breathing-kagome lattice, consistent with the trigonal lattice symmetry of HOF [67]. However, a closer inspection of lattice structure [Fig. 4(a)] finds a perfect kagome lattice with two identical sizes of triangles within the unit cell, while a breathing-kagome

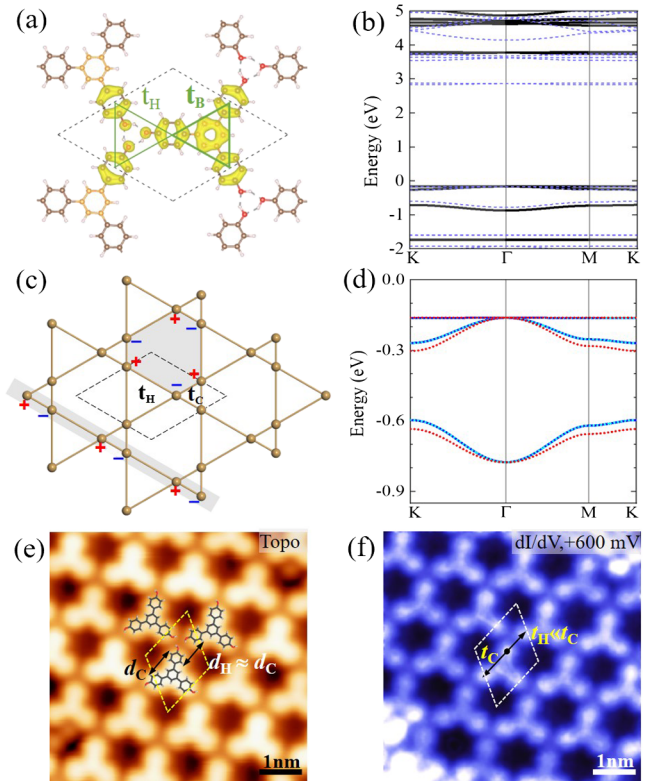


FIG. 4. (a) The optimized lattice structure overlaid with partial charge density derived from the top three valence bands belonging to the breathing-kagome lattice formed by CBRs of THPB. The brown or orange, red, and pink balls represent C, O, and H atoms, respectively. The charge density is plotted using an isosurface of 0.002 $\text{eV}/\text{\AA}^3$. (b) The LDA band structure (blue dashed lines) with a gap corrected by HSE functional (black solid lines). (c) Illustration of an electronic breathing-kagome lattice formed by different hopping strength of t_H via H bonds versus t_C via covalent bonds [see also (a)], as if there were breathing bonds of different lengths. (d) The fit of the top three DFT valence bands (blue solid lines) by the TB breathing-kagome lattice model (red dotted lines) and Wannier bases (cyan dotted lines). (e) Topographic STM image and (f) differential conductance (dI/dV) mapping taken simultaneously at $+600$ meV, using $V_B = -200$ mV, $I_T = 300$ pA, and a bias modulation of 5 mV.

lattice has two triangles of different size, as if one breathes outward and the other inward [Fig. 4(c)] [67]. To resolve this inconsistency, we plot the charge density of the designated three bands overlaid on the lattice in Fig. 4(a), which are mainly contributed by C and O p_z orbitals (Fig. S6 in SM [37]). Then, we uncovered that a sublattice of effectively breathing-kagome type is formed by three CBRs of THPB molecules via two different inter-CBR hopping, namely the H bonds mediated by O and H atoms versus the covalent bonds mediated by the center benzene ring in THPB. Consequently, an interesting scenario of “a breathing-kagome lattice without breathing” is materialized, with the effect of breathing achieved

electronically by different lattice hopping strength via H bond (t_H) and covalent bond (t_C) for the same bond length, as indicated in Fig. 4(a) and illustrated in Fig. 4(c).

To further confirm the above identification of FBs, we have fit the three DFT LDA bands of interest with a tight-binding (TB) breathing-kagome lattice Hamiltonian, as shown in Fig. 4(d). One sees that the TB bands (red dotted lines) agree well with the DFT bands (blue solid lines) using two fitting parameters of $t_H = 0.05$ eV and $t_C = 0.26$ eV, and the former is much smaller than the latter, indicating a strong electronic breathing effect. The fact that the experimentally observed FB is flat over the whole BZ with a singular touching point with a dispersive band indicates it is topological nontrivial [4,5]. In contrast, trivial FB of localized molecular orbitals is usually not flat over the whole BZ and/or isolated without a singular band touching point. This is further supported by a good agreement between the observed bands with theoretical bands whose topological properties are directly calculated. Using the TB model, we calculated the compact localized state and noncontractible loop state in real space to illustrate nontrivial FB topology, which is also confirmed by calculation of topological invariant in k space (Fig. S6 in SM [37]). Moreover, we made Wannier fitting of the DFT LDA bands [cyan dotted lines in Fig. 4(d)], and simulated the ARPES spectra (see Methods and Fig. S7 in SM [37]). The Wannier band dispersions along three paths, Γ to K_{HOF} , Γ to K_{Au} , and $M_{\text{HOF}}-\Gamma_{\text{HOF}}-M_{\text{HOF}}$, are calculated as black dashed lines overlaid on the experimental spectra in Figs. 3(b)–3(d), respectively. Note that we used DFT LDA results for fitting the three breathing-kagome bands because their band dispersions agree better than HSE bands with experiments after aligning the positions of FB. Qualitatively, either LDA or HSE bands confirm the origin of FB from a breathing-kagome lattice.

Further experimental evidence of H bond and breathing-kagome lattice.—To better resolve the H bond, we performed differential conductance (dI/dV) mapping along with STM imaging, to visualize the local charge DOS. Figures 4(e) and 4(f) show the topographic STM image and the dI/dV image, respectively. One sees that the local DOS of covalent C—C bonds bridging the CBRs within a THBP molecule is much higher than that of H bonds bridging the CBRs in between the THBP molecules. This again indicates that the sublattice of all CBRs forms an effective breathing-kagome hopping pattern, as the intra-THBP CBR-CBR hopping [t_C in Fig. 4(f)] via covalent bonds is much stronger than the inter-THBP CBR-CBR hopping [t_H in Fig. 4(f)] via H bonds, although the intra-THBP CBR-CBR distance ($d_C = 7.4$ Å) is about the same as the inter-THBP CBR-CBR distance ($d_H = 7.2$ Å), as shown in Fig. 4(e). This confirms an electronic breathing-kagome lattice without *atomic* breathing bonds. Additional evidence for H bonds is collected from *in situ* Raman spectroscopic measurement (Fig. S4 in SM [37]), supported by DFT phonon calculations (Fig. S9 in SM [37]).

Conclusion.—We demonstrate successful growth of self-assembled mesoscale, highly ordered, and uniform monolayer THPB HOF films, which has enabled observation of a topological FB. DFT calculations reveal the FB to be originated from a hidden electronic breathing-kagome lattice without atomic breathing bonds. Our findings pave the way to future realization of 2D topological and FB materials by the demonstrated approach of self-assembly of HOFs, for which a wide range of molecular precursors and substrates can be explored.

M. P., X. Z., and F. Li acknowledge financial support from the National Natural Science Foundation of China (11574095, 91745115, 22102129, and 11634007). Y. Z., X. Li, and F. Liu acknowledge financial support from U.S. DOE-BES (No. DE-FG02-04ER46148). F. Li also acknowledges financial support from the Suzhou Science and Technology Program (Grant No. SJC2021009) and the Youth Innovation Promotion Association of Chinese Academy of Sciences (2017370). Sample growth, Raman, and ARPES measurements were conducted at the Vacuum Interconnected Nano-X Research Facility in SINANO, Suzhou. STM work was conducted at School of Physics, Huazhong University of Science and Technology in Wuhan. The calculation was done on the CHPC at the University of Utah and U.S.-DOE-NERSC.

*These authors contributed equally to this work.

[†]minghupan@snnu.edu.cn

[‡]jianzhigao@snnu.edu.cn

[§]fsli2015@sinano.ac.cn

^{||}fliu@eng.utah.edu

- [1] A. Mielke, Ferromagnetism in the Hubbard model on line graphs and further considerations, *J. Phys. A* **24**, 3311 (1991).
- [2] A. Mielke, Ferromagnetic ground-states for the Hubbard-model on line graphs, *J. Phys. A* **24**, L73 (1991).
- [3] Z. Liu, F. Liu, and Y.-S. Wu, Exotic electronic states in the world of flat bands: From theory to material, *Chin. Phys. B* **23**, 077308 (2014).
- [4] D. L. Bergman, C. Wu, and L. Balents, Band touching from real-space topology in frustrated hopping models, *Phys. Rev. B* **78**, 125104 (2008).
- [5] J.-W. Rhim and B.-J. Yang, Classification of flat bands According to the band-crossing singularity of Bloch wave functions, *Phys. Rev. B* **99**, 045107 (2019).
- [6] J. Ma, J. W. Rhim, L. Tang, S. Xia, H. Wang, X. Zheng, S. Xia, D. Song, Y. Hu, Y. Li, B. J. Yang, D. Leykam, and Z. Chen, Direct Observation of Flatband Loop States Arising from Nontrivial Real-Space Topology, *Phys. Rev. Lett.* **124**, 183901 (2020).
- [7] E. Tang, J. W. Mei, and X. G. Wen, High-Temperature Fractional Quantum Hall States, *Phys. Rev. Lett.* **106**, 236802 (2011).
- [8] H. Liu, G. Sethi, S. Meng, and F. Liu, Orbital design of flat bands in non-line-graph lattices via line-graph wave functions, *Phys. Rev. B* **105**, 085128 (2022).

- [9] D. Călugăru, A. Chew, L. Elcoro, Y. Xu, N. Regnault, Z.-D. Song, and B. A. Bernevig, General construction and topological classification of crystalline flat bands, *Nat. Phys.* **18**, 185 (2022).
- [10] G. R. Stewart, Non-Fermi-liquid behavior in *d*- and *f*-electron metals, *Rev. Mod. Phys.* **73**, 797 (2001).
- [11] D. Yu, E. M. Lupton, H. J. Gao, C. Zhang, and F. Liu, A unified geometric rule for designing nanomagnetism in graphene, *Nano Res.* **1**, 497 (2008).
- [12] R. Bistritzer and A. H. MacDonald, Moire bands in twisted double-layer graphene, *Proc. Natl. Acad. Sci. U.S.A.* **108**, 12233 (2011).
- [13] C. Wu, D. Bergman, L. Balents, and S. Das Sarma, Flat Bands and Wigner Crystallization in the Honeycomb Optical Lattice, *Phys. Rev. Lett.* **99**, 070401 (2007).
- [14] W. Jiang, H. Huang, and F. Liu, A Lieb-like lattice in a covalent-organic framework and its Stoner ferromagnetism, *Nat. Commun.* **10**, 2207 (2019).
- [15] S. Miyahara, S. Kusuta, and N. Furukawa, BCS theory on a flat band lattice, *Physica (Amsterdam)* **460–462C**, 1145 (2007).
- [16] G. Sethi, Y. Zhou, L. Zhu, L. Yang, and F. Liu, Flat-Band-Enabled Triplet Excitonic Insulator in a Diatomic Kagome Lattice, *Phys. Rev. Lett.* **126**, 196403 (2021).
- [17] Y. Cao, V. Fatemi, S. Fang, K. Watanabe, T. Taniguchi, E. Kaxiras, and P. Jarillo-Herrero, Unconventional superconductivity in magic-angle graphene superlattices, *Nature (London)* **556**, 43 (2018).
- [18] Z. Liu, Z.-F. Wang, J.-W. Mei, Y.-S. Wu, and F. Liu, Flat Chern Band in a Two-Dimensional Organometallic Framework, *Phys. Rev. Lett.* **110**, 106804 (2013).
- [19] Z. F. Wang, N. Su, and F. Liu, Prediction of a two-dimensional organic topological insulator, *Nano Lett.* **13**, 2842 (2013).
- [20] T. Kambe, R. Sakamoto, T. Kusamoto, T. Pal, N. Fukui, K. Hoshiko, T. Shimojima, Z. Wang, T. Hirahara, K. Ishizaka, S. Hasegawa, F. Liu, and H. Nishihara, Redox control and high conductivity of nickel bis(dithiolene) complex pi-nanosheet: A potential organic two-dimensional topological insulator, *J. Am. Chem. Soc.* **136**, 14357 (2014).
- [21] W. Jiang, X. Ni, and F. Liu, Exotic topological bands and quantum states in meta organic and covalent-organic frameworks, *Acc. Chem. Res.* **54**, 416 (2021).
- [22] B. Cui, X. Zheng, J. Wang, D. Liu, S. Xie, and B. Huang, Realization of Lieb lattice in covalent-organic frameworks with tunable topology and magnetism, *Nat. Commun.* **11**, 66 (2020).
- [23] X. Ni, H. Li, F. Liu, and J. L. Bredas, Engineering of flat bands and Dirac bands in two-dimensional covalent organic frameworks (COFs): Relationships among molecular orbital symmetry, lattice symmetry, and electronic-structure characteristics, *Mater. Horiz.* **9**, 88 (2022).
- [24] Y. Jing and T. Heine, Making 2D topological polymers a reality, *Nat. Mater.* **19**, 823 (2020).
- [25] S. Ghosh, Y. Tsutsui, T. Kawaguchi, W. Matsuda, S. Nagano, K. Suzuki, H. Kaji, and S. Seki, Band-like transport of charge carriers in oriented two-dimensional Conjugated covalent organic frameworks, *Chem. Mater.* **34**, 736 (2022).
- [26] C.-H. Liu, A. Wei, M. F. Cheung, and D. F. Perepichka, Vanishing electronic band gap in two-dimensional hydrogen-bonded organic frameworks, *Chem. Mater.* **34**, 3461 (2022).
- [27] H. Liu, S. Meng, and F. Liu, Screening two-dimensional materials with topological flat bands, *Phys. Rev. Mater.* **5**, 084203 (2021).
- [28] Z. Lin, J. H. Choi, Q. Zhang, W. Qin, S. Yi, P. Wang, L. Li, Y. Wang, H. Zhang, Z. Sun, L. Wei, S. Zhang, T. Guo, Q. Lu, J. H. Cho, C. Zeng, and Z. Zhang, Flatbands and Emergent Ferromagnetic Ordering in Fe₃Sn₂ Kagome Lattices, *Phys. Rev. Lett.* **121**, 096401 (2018).
- [29] Y. Yang, Q. Wan, J. P. Song, Z. Du, J. Tang, Z. W. Wang, N. C. Plumb, M. Radovic, G. W. Wang, G. Y. Wang *et al.*, Evidence of orbit-selective electronic Kagome lattice with planar flat-band in correlated paramagnetic YCr₆Ge₆, *Quantum Front.* **1**, 14 (2022).
- [30] Z. Liu, M. Li, Q. Wang, G. Wang, C. Wen, K. Jiang, X. Lu, S. Yan, Y. Huang, D. Shen, J. X. Yin, Z. Wang, Z. Yin, H. Lei, and S. Wang, Orbital-selective Dirac fermions and extremely flat bands in frustrated kagome-lattice metal CoSn, *Nat. Commun.* **11**, 4002 (2020).
- [31] M. Kang, S. Fang, L. Ye, H. C. Po, J. Denlinger, C. Jozwiak, A. Bostwick, E. Rotenberg, E. Kaxiras, J. G. Checkelsky, and R. Comin, Topological flat bands in frustrated kagome lattice CoSn, *Nat. Commun.* **11**, 4004 (2020).
- [32] M. Li, Q. Wang, G. Wang, Z. Yuan, W. Song, R. Lou, Z. Liu, Y. Huang, Z. Liu, H. Lei, Z. Yin, and S. Wang, Dirac cone, flat band and saddle point in kagome magnet YMn₆Sn₆, *Nat. Commun.* **12**, 3129 (2021).
- [33] M. Kang *et al.*, Dirac fermions and flat bands in the ideal kagome metal FeSn, *Nat. Mater.* **19**, 163 (2020).
- [34] S. Lisi *et al.*, Observation of flat bands in twisted bilayer graphene, *Nat. Phys.* **17**, 189 (2021).
- [35] T. Yilmaz, X. Tong, Z. Dai, J. T. Sadowski, E. F. Schwier, K. Shimada, S. Hwang, K. Kisslinger, K. Kaznatcheev, E. Vescovo, and B. Sinkovic, Emergent flat band electronic structure in a VSe₂/Bi₂Se₃ heterostructure, *Commun. Mater.* **2**, 11 (2021).
- [36] G. Galeotti, F. De Marchi, E. Hamzehpoor, O. MacLean, M. Rajeswara Rao, Y. Chen, L. V. Besteiro, D. Dettmann, L. Ferrari, F. Frezza, P. M. Sheverdyaeva, R. Liu, A. K. Kundu, P. Moras, M. Ebrahimi, M. C. Gallagher, F. Rosei, D. F. Perepichka, and G. Contini, Synthesis of mesoscale ordered two-dimensional π -conjugated polymers with semiconducting properties, *Nat. Mater.* **19**, 874 (2020).
- [37] See Supplemental Material at <http://link.aps.org/supplemental/10.1103/PhysRevLett.130.036203> for supplemental text and Figs. S1–S10, which includes Refs. [28,38–56].
- [38] I. Horcas, R. Fernandez, J. M. Gomez-Rodriguez, J. Colchero, J. Gomez-Herrero, and A. M. Baro, WSXM: A software for scanning probe microscopy and a tool for nanotechnology, *Rev. Sci. Instrum.* **78**, 013705 (2007).
- [39] J. P. Perdew and A. Zunger, Self-interaction correction to density-functional approximations for many-electron systems, *Phys. Rev. B* **23**, 5048 (1981).
- [40] J. Heyd and G. E. Scuseria, Erratum: “Hybrid functionals based on a screened Coulomb potential” [J. Chem. Phys. **118**, 8207 (2003)], *J. Chem. Phys.* **122**, 234102 (2005).

- [41] J. Paier, M. Marsman, and G. Kresse, Why does the B3LYP hybrid functional fail for metals?, *J. Chem. Phys.* **127**, 024103 (2007).
- [42] G. Kresse and J. Furthmüller, Efficient iterative schemes for ab initio total-energy calculations using a plane-wave basis set, *Phys. Rev. B* **54**, 11169 (1996).
- [43] M. Methfessel and A. T. Paxton, High-precision sampling for Brillouin-zone integration in metals, *Phys. Rev. B* **40**, 3616 (1989).
- [44] D. Hobbs, G. Kresse, and J. Hafner, Fully unconstrained noncollinear magnetism within the projector augmented-wave method, *Phys. Rev. B* **62**, 11556 (2000).
- [45] Q. Wu, S. Zhang, H.-F. Song, M. Troyer, and A. A. Soluyanov, WannierTools: An open-source software package for novel topological materials, *Comput. Phys. Commun.* **224**, 405 (2018).
- [46] N. Marzari and D. Vanderbilt, Maximally localized generalized Wannier functions for composite energy bands, *Phys. Rev. B* **56**, 12847 (1997).
- [47] A. Farrell, A. Arsenault, and T. Pereg-Barnea, Dirac cones, Floquet side bands, and theory of time-resolved angle-resolved photoemission, *Phys. Rev. B* **94**, 155304 (2016).
- [48] M. A. Sentef, M. Claassen, A. F. Kemper, B. Moritz, T. Oka, J. K. Freericks, and T. P. Devereaux, Theory of Floquet band formation and local pseudospin textures in pump-probe photoemission of graphene, *Nat. Commun.* **6**, 7047 (2015).
- [49] J. K. Freericks, H. R. Krishnamurthy, and T. Pruschke, Theoretical Description of Time-Resolved Photoemission Spectroscopy: Application to Pump-Probe Experiments, *Phys. Rev. Lett.* **102**, 136401 (2009).
- [50] N. Koch, Energy levels at interfaces between metals and conjugated organic molecules, *J. Phys. Condens. Matter* **20**, 184008 (2008).
- [51] A. Franco-Cañellas, S. Duhm, A. Gerlach, and F. Schreiber, Binding and electronic level alignment of π -conjugated systems on metals, *Rep. Prog. Phys.* **83**, 066501 (2020).
- [52] Y. Ling, W. C. Xie, G. K. Liu, R. W. Yan, Y. Wu, and J. Tang, The discovery of the hydrogen bond from *p*-Nitrothiophenol by Raman spectroscopy: Guideline for the thioalcohol molecule recognition tool, *Sci. Rep.* **6**, 31981 (2016).
- [53] T. Korzdorfer, S. Kummel, N. Marom, and L. Kronik, When to trust photoelectron spectra from Kohn-Sham eigenvalues: The case of organic semiconductors, *Phys. Rev. B* **79**, 201205(R) (2009).
- [54] A. Haags *et al.*, Momentum space imaging of π orbitals for chemical analysis, *Sci. Adv.* **8**, eabn0819 (2022).
- [55] M. Preuss and F. Bechstedt, Vibrational spectra of ammonia, benzene, and benzene adsorbed on Si(001) by first principles calculations with periodic boundary conditions, *Phys. Rev. B* **73**, 155413 (2006).
- [56] L. D. Ziegler and B. Hudson, Resonance Raman scattering of benzene and benzene- d_6 with 212.8 nm excitation, *J. Chem. Phys.* **74**, 982 (1981).
- [57] A. C. Marele, I. Corral, P. Sanz, R. Mas-Ballesté, F. Zamora, M. Yáñez, and J. M. Gómez-Rodríguez, Some pictures of alcoholic dancing: From simple to complex hydrogen-bonded networks based on polyalcohols, *J. Phys. Chem. C* **117**, 4680 (2013).
- [58] Q. Li, B. Yang, H. Lin, N. Aghdassi, K. Miao, J. Zhang, H. Zhang, Y. Li, S. Duhm, J. Fan, and L. Chi, Surface-controlled mono/diselective ortho C—H bond activation, *J. Am. Chem. Soc.* **138**, 2809 (2016).
- [59] C. Woll, S. Chiang, R. J. Wilson, and P. H. Lippel, Determination of atom positions at stacking-fault dislocations on Au(111) by scanning tunneling microscopy, *Phys. Rev. B* **39**, 7988 (1989).
- [60] G. Koller, S. Berkebile, M. Oehzelt, P. Puschnig, C. Ambrosch-Draxl, F. P. Netzer, and M. G. Ramsey, Intra- and intermolecular band dispersion in an organic crystal, *Science* **317**, 351 (2007).
- [61] S. Ciuchi, R. C. Hatch, H. Hochst, C. Faber, X. Blase, and S. Fratini, Molecular Fingerprints in the Electronic Properties of Crystalline Organic Semiconductors: From Experiment to Theory, *Phys. Rev. Lett.* **108**, 256401 (2012).
- [62] Y. Nakayama, S. Kera, and N. Ueno, Photoelectron spectroscopy on single crystals of organic semiconductors: Experimental electronic band structure for optoelectronic properties, *J. Mater. Chem. C* **8**, 9090 (2020).
- [63] A. Winkelmann, C. Tusche, A. Akin Ünäl, M. Ellguth, J. Henk, and J. Kirschner, Analysis of the electronic structure of copper via two-dimensional photoelectron momentum distribution patterns, *New J. Phys.* **14**, 043009 (2012).
- [64] P. M. Sheverdyeva, R. Requist, P. Moras, S. K. Mahatha, M. Papagno, L. Ferrari, E. Tosatti, and C. Carbone, Energy-momentum mapping of *d*-derived Au(111) states in a thin film, *Phys. Rev. B* **93**, 035113 (2016).
- [65] A. J. Garza and G. E. Scuseria, Predicting band gaps with hybrid density functionals, *J. Phys. Chem. Lett.* **7**, 4165 (2016).
- [66] K. Sun, Z. Gu, H. Katsura, and S. Das Sarma, Nearly Flatbands with Nontrivial Topology, *Phys. Rev. Lett.* **106**, 236803 (2011).
- [67] M. Ezawa, Higher-Order Topological Insulators and Semimetals on the Breathing Kagome and Pyrochlore Lattices, *Phys. Rev. Lett.* **120**, 026801 (2018).